Toward observation of three-nucleon short-range correlations in high-Q^2 $A(e, e')X$ reactions

Donal B. Day,[1] Leonid L. Frankfurt,[2] Misak M. Sargsian,[3] and Mark I. Strikman[4]
[1]*Department of Physics, University of Virginia, Charlottesville, Virginia 22904, USA*
[2]*Sackler School of Exact Sciences, Tel Aviv University, Tel Aviv 69978, Israel*
[3]*Department of Physics, Florida International University, Miami, Florida 33199, USA*
[4]*Department of Physics, Pennsylvania State University, University Park, Pennsylvania 16802, USA*

(Received 23 June 2022; accepted 13 December 2022; published 24 January 2023)

We present a detailed study of the kinematical and dynamical conditions necessary for probing highly elusive three-nucleon short-range correlations (3N-SRCs) in nuclei through inclusive electron scattering. The kinematic requirements that should be satisfied in order to isolate 3N-SRCs in inclusive processes are derived. We demonstrate that a sequence of two short-range NN interactions is the main mechanism for 3N-SRCs in such processes. With this mechanism we predict a quadratic dependence of the cross section ratios of nuclei to ^{3}He in the 3N-SRC region to the same ratio measured in the 2N-SRC domain. An extended analysis of the available data which satisfies the required 3N-SRC kinematical conditions is presented. This analysis reveals tantalizing signatures of the scaling associated with the onset of 3N-SRC dominance. The same data are also consistent with the prediction of the quadratic relation between the ratios measured in the 3N- and 2N-SRC regions for nuclei ranging $4 \leqslant A \leqslant 197$. This agreement made it possible to extract $a_3(A)$, the probability of 3N-SRCs relative to the $A = 3$ nucleus. We find $a_3(A)$ to be significantly larger in magnitude than the analogous parameter, $a_2(A)$, for 2N-SRCs.

DOI: 10.1103/PhysRevC.107.014319

I. INTRODUCTION

For the last several decades there have been intensive studies of two-nucleon short-range correlations (2N-SRCs) in nuclei using both electron [1–7] and proton [8,9] probes in high momentum transfer reactions. Inclusive electron scattering experiments [2,3,6], in which only the scattered electron is detected, established the existence of the scaling properties associated with 2N-SRCs, confirming the observation [1] based on the analysis of SLAC data [10–15]. From these experiments $a_2(A, Z)$, describing the probability of finding 2N-SRC in a given nucleus relative to the deuteron, was extracted. The analysis of $A(p, 2p)X$ data yielded similar estimates for $a_2(A, Z)$ for proton induced reactions [16]. Moreover, the strength of 2N-SRCs found in these analyses agreed with the one obtained from fast backward nucleon production in high energy inclusive $p(\gamma)$-A scattering [17]. The consistency among these measurements of the 2N-SRC strength with different probes supports the conjecture that a genuine property of the nuclear ground state wave function has been probed.

The extension of 2N-SRC studies to semi-inclusive processes in which, in addition to the scattered probe, the struck nucleons [4,5] or both struck and recoil nucleons from 2N-SRCs [8,9] have been detected, discovered the strong (a factor of 20) dominance [5,18] of pn SRCs as compared to pp and nn SRCs in the probed internal momentum range of 300–650 MeV/c. The pn excess is understood [19,20] when considering the dominance of the tensor interaction at internucleon distances of 0.8–1.2 fm and which supports the commanding role of 2N-SRCs in the high momentum component of the nuclear wave function. Based on the pn-SRC dominance it was predicted that the minority component in asymmetric nuclei should have larger kinetic energy [21], which was confirmed experimentally [22–24].

The experimental focus on 2N-SRCs stimulated extensive theoretical efforts (see, e.g., Refs. [17,25–29]) to calculate the multitude of nuclear quantities entering into the cross sections of inclusive and semi-inclusive electron nuclear scattering. Such quantities are the nuclear spectral and decay functions which are based on the 2N-SRC model of the high momentum component of the nuclear ground state wave function.

A question which naturally arises is, what is the structure of the nuclear wave function at even larger internal momenta of the bound nucleons (>650 MeV/c)? One of the important issues in this regard is the possible formation of 3N-SRCs. Understanding the strength and dynamics of 3N-SRCs is essential to advance our knowledge of superdense nuclear matter. In most realistic models of the nuclear equation of state 3N-SRCs play an increasingly important role above the saturation densities (see, e.g., Ref. [30]). The 3N-SRCs can be formed both by nuclear forces that can be reduced to a sequence of two short-range elastic NN interactions and by irreducible 3N forces that contain inelastic transitions in the intermediate state.

Experimental evidence for 3N-SRCs is very limited. One of the main obstacles in isolating and probing 3N-SRCs is that they have a much reduced probability compared to

2N-SRCs. Analysis of Lippmann-Schwinger type equations for nuclear bound states [31,32], strongly suggests that 2N-SRCs dominate the momentum distribution for momenta larger than those characteristic of 2N-SRCs. Thus the study of 3N-SRCs requires the consideration of variables other than just the momentum of the bound nucleon. One such parameter is α [17], the light-cone (LC) momentum fraction of the nucleus carried by the bound nucleon. In collider kinematics α is equal to the ratio of the nucleon longitudinal momentum to the nucleus momentum, scaled by A, such that, in the case of equal partition of the nuclear momentum, $\alpha = 1$. The condition that $\alpha > 2$ requires at least three nucleons to be in close proximity in order for a single nucleon to carry more than two nucleons' momentum fraction. An early analysis of few nucleon SRCs [17] in the backward production of protons with momenta $0.3 < p < 1.5$ GeV/c indicated that the scattering off 3N-SRCs begins to dominate the 2N-SRC contribution starting at $\alpha \simeq 1.6$, which we consider as a kinematic threshold for isolating 3N-SRCs.

In inclusive $A(e, e')X$ reactions it is expected that the dominance of 3N-SRCs will be revealed by the onset of another plateau in the ratios of per-nucleon cross sections of heavy to light nuclei at $x > 2$. However, observation of such a plateau has been elusive. One of the first attempts to isolate 3N-SRC at Bjorken $x > 2$ observed a possible plateau [3], though subsequent measurements of the ratio $\frac{3\sigma_{^4\mathrm{He}}}{4\sigma_{^3\mathrm{He}}}$ did not make that claim [6]. The most recent measurement [33] of the inclusive cross section ratios of ^{4}He to ^{3}He at $x > 2$ and $1.5 < Q^2 < 1.9$ GeV^2 are largely in agreement with Ref. [6] in that no plateau was observed. This situation corroborated the suggestion [34] that poor momentum resolution for the scattered electrons in the experiment of Ref. [3] allowed events to migrate from smaller to larger x bins and was responsible for the appearance of the plateau at $x > 2$.

In the recent work [35] we reported the partial analysis of inclusive $A(e, e')X$ data utilizing the above discussed kinematic variable α for ($\gtrsim$1.6) region. We demonstrated that the data in this domain show a tantalizing signature for another layer of scaling for the ratio of per-nucleon inclusive cross sections $\frac{3\sigma(^4\mathrm{He})}{4\sigma(^3\mathrm{He})}$. The analysis of other nuclei indicated also an agreement with the theoretical prediction of a quadratic proportionality of $a_3(A)$ to the ratio of $\frac{a_2(A)}{a_2(A=3)}$ measured in the 2N SRC domain.

In the current paper we present a detailed theoretical analysis of inclusive scattering at $\alpha > 1$ kinematics and provide a theoretical foundation for the observation of a new layer of nuclear scaling at $\alpha > \alpha^0_{3N}$ as well as the expectation of a quadratic proportionality between the probabilities of 2N- and 3N-SRCs. We also present a more complete analysis of the experimental data of Ref. [6,36] using varied approaches to treat the poor quality of the cross section at large x, expected to be dominated by 3N-SRCs.

In Sec. II we elaborate on the kinematics of 3N-SRCs using the variable α that characterizes the light-cone momentum fraction of the nucleus carried by the bound nucleon. By analyzing the decay function of the ^{3}He nucleus we identify the dominant mechanism forming 3N-SRCs in inclusive eA scattering and, within this picture, calculate the LC momentum fraction, α_{3N}, corresponding to scattering from a nucleon in 3N-SRC. This variable allows us to identify the optimal kinematics for probing 3N-SRCs in inclusive scattering. Section III discusses the dynamical origin of 3N-SRCs. Based on the model in which 3N-SRCs are generated through the two successive pn short-range interactions it is predicted that the light-cone nuclear density matrix which enters in the $A(e, e')X$ cross section is proportional to the convolution of two pn-SRC density functions. In Sec. IV final state interactions in inclusive processes are considered as a potential source masquerading or destroying 3N-SRCs. Here we employ the important property of high energy small angle scattering where the quantity α is approximately conserved in rescattering processes. An experimental observable of 3N-SRCs in $A(e, e')X$ reactions is presented in Sec. V, where we also derive the quadratic relation between the ratios of inclusive cross sections measured in the 3N- and 2N-SRC regions. Section VI presents the analysis of the existing inclusive data in light of the theoretical considerations presented in the previous sections. In Sec. VII we summarize our results and give an outlook on the perspective of unambiguous verification of 3N SRCs.

II. DEFINITION OF 2N- AND 3N-SRCs

In a nonrelativistic formulation we define a nucleon to be in a 2N-SRC pair if its momentum exceeds the characteristic nuclear Fermi momentum ($k_F \approx 250$ MeV/c) and is almost completely balanced by the momentum of the correlated nucleon in the pair. In the light-cone representation the requirement is that LC momentum fractions of the correlated nucleons α_1 and α_2 satisfy the conditions $\alpha_i \geqslant 1.3$ or $\alpha_i \leqslant 0.7$ for $i = 1, 2$ and $\alpha_1 + \alpha_2 \approx 2$. There are also 2N-SRCs with $\alpha_i \approx 1$ and $p_\perp > 0.3$ GeV/c; however, they are not important for inclusive scattering at $x > 1$.

For the nucleon in a 3N-SRC we assume again that its momentum significantly exceeds k_F, but in this case this momentum is balanced by two correlated nucleons each with momenta exceeding k_F. As in the case of 2N-SRCs the center-of-mass momentum of the 3N-SRC is small, $p_{cm} \leqslant k_F$. The description of 3N-SRCs in the LF representation corresponds to the situation in which $\alpha_i \geqslant 1.3$ or $\alpha_i \leqslant 0.7$ for $i = 1, 2, 3$ and $\alpha_1 + \alpha_2 + \alpha_3 \approx 3$. Similarly to 2N-SRC case, some 3N correlations may correspond to the kinematics in which $\alpha_i \approx 1$ with nucleons having very large transverse momenta. We do not discuss here such correlations since they contribute very little to $A(e, e')X$ reactions at $x > 1$.

The complete nuclear wave function should incorporate components related to 2N- and 3N-SRCs. However, the first-principles calculation of a wave function containing these components is currently impossible due to a poor understanding of strong interaction dynamics at short internucleon distances. Relativistic effects that become increasingly important at large momenta of nucleons involved in short-range correlations are also an impediment.

In this respect the progress can be achieved by experimental studies of 3N-SRCs, which are currently becoming more accessible with the 12 GeV energy upgrade of Jefferson Lab. One way of addressing the problem of experimentally

isolating 3N-SRCs, is a proper identification of the experimentally determined variables that can unambiguously discriminate 3N- from 2N-SRCs. As was mentioned in the Introduction, the relevant variable is the light-cone momentum fraction of the nucleus carried by the interacting bound nucleon, α, first suggested in Refs. [17,37]. The α variable, in the reference frame in which the nucleus has a large momentum in the $-z$ direction, is defined as[1]

$$\alpha = A\frac{E_N - k_{N,z}}{E_A - k_{A,z}}, \tag{1}$$

where $(E_A, k_{A,z})$ and $(E_N, k_{N,z})$ are the energy and longitudinal momentum of the nucleus and bound nucleon respectively in the noncovariant LF nuclear wave function.

It was first suggested in Ref. [17] that, due to the short-range nature of nuclear forces, when

$$j - 1 < \alpha < j, \tag{2}$$

where $j > 2$, the scattering from j-nucleon SRC from the nucleus will be ensured. However, the fact that the probability of a j-nucleon SRC in finite nuclei is $\approx (\frac{r_{NN}}{r_{AV}})^{3(j-1)}$ with a correlation length $r_{NN} \ll r_{AV}$, where r_{AV} is the average internucleon distance, suggests that the transition from j to the $j+1$ SRC should occur at somewhat smaller $\alpha \lesssim j$ [17]. The latter inequality means that 3N-SRCs begin to dominate at $\alpha \simeq 2$.

A. 2N SRCs

In 1993, guided by Eq. (2), we studied the possibility of exposing 2N-SRCs in high Q^2 inclusive $A(e,e')X$ reactions [1] by identifying the relevant light-cone momentum fraction α_{2N} for inclusive processes as

$$\alpha_{2N} = 2 - \frac{q_- + 2m_N}{2m_N}\left(1 + \frac{\sqrt{W_{2N}^2 - 4m_N^2}}{W_{2N}}\right), \tag{3}$$

where $q_- = q_0 - |\mathbf{q}|$ and $W_{2N}^2 = (q + 2m_N)^2 = -Q^2 + 4q_0 m_N + 4m_N^2$, with m_N the nucleon mass, q_0 and $\mathbf{q}$ representing energy and momentum transfer, and $Q^2 = \mathbf{q}^2 - q_0^2$. Eq. (3) explicitly takes into account the recoil energy and momentum carried by the spectator nucleon in the 2N-SRC and ensures that solutions for α_{2N} exist only for $x \leqslant 2$, where $x = \frac{Q^2}{2m_N q_0}$ is the Bjorken variable. Additionally, in the limit of large Q^2, $\alpha_{2N} \approx x$, and the variable x can replace α_{2N} for identification of 2N-SRCs in the large Q^2 limit.

One of the important advantages of the LF treatment is that the inclusive scattering cross section can be factorized into the electron-bound nucleon scattering cross section, σ_{eN}, and light cone density matrix, $\rho_A(\alpha_{2N})$, in the following form [17,38]:

$$\sigma_{eA} \approx \sum_N \sigma_{eN}\rho_A(\alpha_{2N}). \tag{4}$$

[1]This variable has a equivalence with Bjorken x_{Bj} that describes the light-cone momentum fraction of the nucleon carried by a parton.

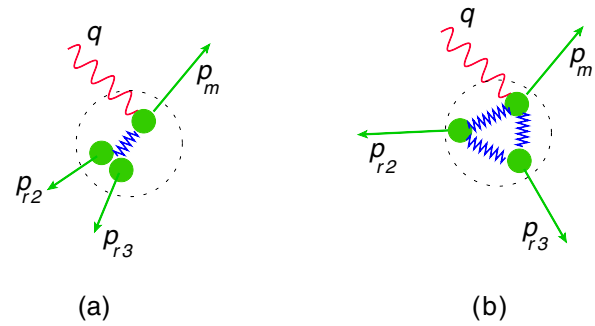

FIG. 1. Types of three nucleon SRCs. (a) In type 3N-I SRC the fast probed nucleon is balanced by two recoil nucleons with momenta $\approx p_m/2$. (b) In type 3N-II SRC all tree nucleons have equal momenta with relative angles $\approx 120^\circ$.

Note that within a nonrelativistic framework no such simple factorization exists and the inclusive cross section is expressed through an integral over $p_m^\perp$ and E_m of the convolution of σ_{eN} and the nuclear spectral function, $S_A(p_m, E_m)$, where p_m and E_m are the missing momentum and energy in the reaction (see, e.g., Refs. [38,39]). The theoretical justification for the factorization in Eq. (4) in the high Q^2 limit, is based on the validity of the closure approximation over the "plus" component, p_+, of the four-momentum of the bound nucleon in LF the formalism (see, e.g., Ref. [38]). The p_+ component in the LF formalism is analogous to the missing energy E_m and in the calculation of σ_{eN} it is estimated at the average point, corresponding to the 2N-SRC at rest, $p_+ \approx 2m_N - \frac{m_N}{2-\alpha_{2N}}$. Based on Eqs. (4) and (2) we predicted [1] that, due to the dominance of 2N-SRC dynamics, the per-nucleon ratios of inclusive cross sections of nuclei and the deuteron,

$$a_2(A,Z) = \frac{2\sigma_{eA}(\alpha_{2N}, Q^2)}{A\sigma_{ed}(\alpha_{2N}, Q^2)}, \tag{5}$$

should scale with α_{2N} for $1.3 < \alpha_{2N} < 2$ and $Q^2 > 1.5\ \mathrm{GeV}^2$, with the parameter $a_2(A,Z)$ representing the probability of finding a 2N-SRC in nucleus A relative to the deuteron. Here, the lower limit of α_{2N} corresponds to the scattering off a bound nucleon with average momentum of $p \gtrsim 0.3\ \mathrm{GeV}/c$.

The analysis of the available data [1] at that time from large Q^2 inclusive experiments at SLAC was in agreement with the prediction of the scaling in Eq. (5). Subsequent dedicated experiments [2,3,6] at JLab confirmed this prediction and obtained similar estimates for the scaling parameter $a_2(A,Z)$ for the wide range of atomic nuclei A (see, e.g., Fig. 10 and the related discussion in Sec. VI.).

B. 3N-SRCs

For 2N-SRCs we considered the only possible configuration in which two fast nucleons are correlated back to back with a small center-of-mass momentum. For 3N-SRCs, however, there are more configurations in which three fast nucleons have small center-of-mass momentum. Two extreme cases of possible 3N-SRC configurations are presented in Fig. 1. The first, Fig. 1(a), referred as type 3N-I SRC, corresponds to the situation in which the probed fast nucleon is

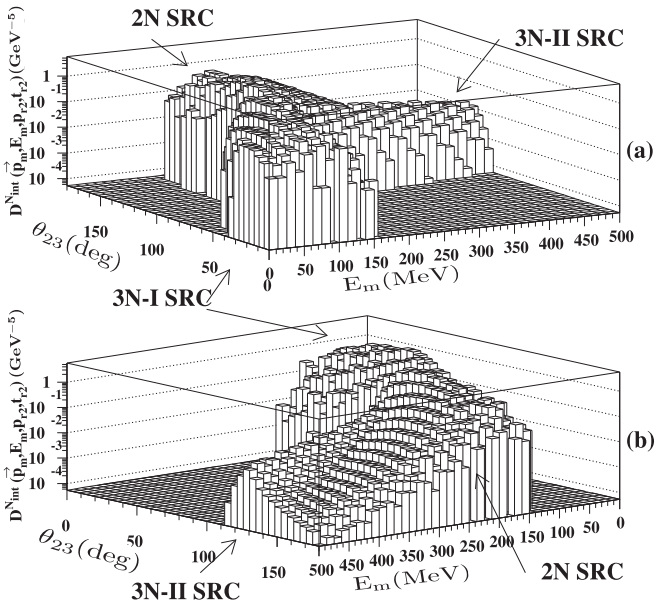

FIG. 2. Decay function for the ^{3}He nucleus calculated with the condition $p_m \geqslant 700$ MeV/c, and $p_{r2}, p_{r3} \geqslant k_F$. The θ_{23} is the relative angle between two recoil nucleons and E_m is the missing energy. The two panels show different points of view of the same figure. The figure is adapted from Ref. [19].

balanced by two fast spectator nucleons $p_{r2}, p_{r3} \sim p_m/2$ with a small relative angle between them, thus a small invariant mass $m_S \sim 2m_N$. The second case, Fig. 1(b), corresponds to the symmetric situation in which all three nucleons have comparable momenta with relative angles $\theta_{23} \approx 120^\circ$.

To determine which of these 3N-SRC configurations will dominate in inclusive $A(e, e')X$ scattering it is instructive to consider the decay function for a three-body nucleus at large values of missing and recoil momenta, noticing that it is the integrated decay function which enters in the cross section of inclusive scattering. The decay function has been calculated in Refs. [19,40] for ^{3}He using a realistic wave function based on the solution of Faddeev equations [41] and one of the results relevant for 3N-SRCs is presented in Fig. 2. In the figure a correlation between the relative angle of two recoil nucleons, θ_{23}, and missing energy E_m is presented for $p_m \geqslant 700$ MeV/c and $p_{r2}, p_{r3} > k_F$. As the figure shows, the type 3N-I SRC provides the dominant contribution to the decay function at small missing energies, $E_m \sim \frac{p^2}{4m_N}$, with the relative angle between spectator nucleons $\theta_{23} \leqslant 50^\circ$ [see Fig. 2(a)]. A transition to the type 3N-II SRC is observed with an increase of missing energy $E_m \geqslant 200$ MeV, in which case $\theta_{23} \approx 120^\circ$. The analysis of type 3N-II SRCs [19] demonstrates that the irreducible three-nucleon forces have substantial contribution in this region due to large missing energies, which increases the possibility of an inelastic $N \to \Delta$ transition at the NN vertices of the correlation.

Since the integrated decay function, which enters in the inclusive cross section, is dominated by smaller values of E_m, one expects, based on the above discussion, that the type 3N-I SRC represents the main configuration contributing to the inclusive cross section. Based on this, it is possible to identify the kinematics at which 3N-SRCs can be isolated in inclusive scattering. Introducing mass m_S and momentum p_S for the two-nucleon recoil system of type 3N-I SRC [Fig. 1(a)], we consider energy-momentum conservation in quasielastic scattering from a 3N-SRC, which takes the form

$$q + 3m_N = p_f + p_S. \tag{6}$$

Here q is the four-momentum transfer and p_f is the final four-momentum of the struck nucleon in the 3N SRC. The boost invariance of the light-cone momentum fractions, for the spectator system in the $\gamma - 3N$ center of mass frame, allows us to define the ratio

$$\frac{p_s^-}{p_{\gamma 3N}^-} = \frac{E_S^{cm} + p_{S,z}^{cm}}{E_S^{cm} + E_f^{cm}} \approx \frac{E_S^{cm} + p_S^{cm}}{W_{3N}}, \tag{7}$$

where W_{3N} is the invariant mass produced from the interaction with the 3N system:

$$W_{3N}^2 = (q + 3m_N)^2 = Q^2 \frac{3 - x}{x} + 9m_N^2. \tag{8}$$

In the right-hand side of Eq. (7) we neglected the transverse momentum of the spectator NN system as it is integrated over in inclusive reactions. This is justified since the inclusive cross section is dominated by kinematics in which $p_{S,\perp} \ll p_{S,z}$. Furthermore E_S^{cm} and p_S^{cm} can be calculated through W_{3N} using the relations

$$E_S^{cm} = \frac{W_{3N}^2 - m_N^2 + m_S^2}{2W_{3N}} \quad \text{and} \quad p_S^{cm} = \sqrt{E_S^{cm,2} - m_S^2}, \tag{9}$$

where m_S is defined as

$$m_S^2 = 4\frac{m_N^2 + k_\perp^2}{\beta(2 - \beta)}, \tag{10}$$

with $k_\perp$ being the transverse component of the relative momentum of the spectator nucleons with respect to $\vec{p}_S$. β is the light-cone momentum fraction of p_S carried by one of the spectator nucleons and is scaled to be $0 \leqslant \beta \leqslant 2$.

Equation (7) can be used to estimate the light-cone momentum fraction of the nucleon in a 3N-SRC by observing that $\alpha_{3N} = 3 - \alpha_S$, where $\alpha_S = 3\frac{p_S^-}{p_{3N}^-}$:

$$\alpha_{3N} = 3 - 3\frac{p_S^-}{p_{3N}^-} = 3 - 3\frac{p_S^-}{p_{\gamma 3N}^-}\frac{p_{\gamma 3N}^-}{p_{3N}^-}, \tag{11}$$

where we again exploit the boost invariance of the ratio of $\frac{p_{\gamma 3N}^-}{p_{3N}^-} = \frac{q_- + 3m_N}{3m_N}$ along $\mathbf{q}$. This results in the following expression for the light-cone momentum fraction of the nucleon with the largest momentum belonging to 3N-SRCs:

$$\alpha_{3N} = 3 - \frac{q_- + 3m_N}{2m_N}\left[1 + \frac{m_S^2 - m_N^2}{W_{3N}^2} + \sqrt{\left(1 - \frac{(m_S + m_n)^2}{W_{3N}^2}\right)\left(1 - \frac{(m_S - m_n)^2}{W_{3N}^2}\right)}\right]. \tag{12}$$

Using this equation we can identify the kinematical conditions for x and Q^2 for which the inclusive cross section is dominated by scattering from a nucleon in a 3N-SRC. For this, we first

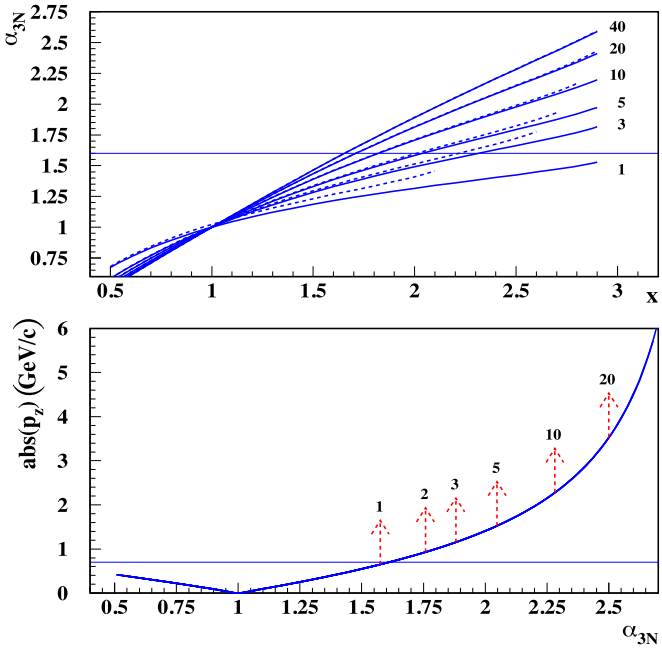

FIG. 3. Kinematics of 3N-SRCs. Upper panel: Relation between α_{3N} and x for m_S calculated according to Eq. (10) with $k = 0$ (dotted line) and $k = 250$ MeV/c (dashed line). The curves are labeled by their respective Q^2 values. Lower panel: The dependence of $|p_z|$ on α_{3N}. Arrows indicate the maximum possible α_{3N}'s that can be reached at given values of Q^2.

need to determine the threshold value, α^0_{3N}, above which one expects the onset of 3N-SRC dynamics. We also need an estimate of m_S through Eq. (10). We note that for inclusive $A(e, e')X$ scattering the cross section is defined by the nuclear light-cone density matrix where one integrates over the range of the two-nucleon spectator system masses $m_S \geqslant 2m_N$. This integral, however, is dominated by $\beta \approx 1$ with the recoil nucleon's momentum, k relative to p_S not exceeding the nuclear Fermi momentum, $k_F \approx 250$ MeV/c (see, e.g., Ref. [19]). For numerical estimates we consider two values for k: $k = 0$ and $k = 250$ MeV/c.

With these considerations and Eq. (12) we are able to identify the most favorable domain in x and Q^2 to search for 3N-SRCs in inclusive $A(e, e')X$ reactions. In Fig. 3 (upper panel) we present the α_{3N}-x relation for different values of Q^2. The solid and dashed curves correspond to the spectator mass, m_S calculated according to Eq. (10) with $k = 0$ and $k = 250$ MeV/c. Figure 3 shows that at $Q^2 \approx 3$ GeV^2 there exists a finite kinematic domain with $\alpha_{3N} \geqslant 1.6$, where one expects the onset of the 3N-SRC dominance. In addition, starting with $Q^2 \geqslant 5$ GeV^2 the onset of 3N-SRCs is practically insensitive to the recoil mass of the spectator system, m_S. As follows from the figure, for $Q^2 \gtrsim 3$ and 5 GeV^2 the magnitudes of $x \gtrsim 2.2$ and $x \gtrsim 2$ respectively are necessary to probe $\alpha_{3N} > 1.6$. Furthermore, using the relation

$$\alpha_S = 3 - \alpha_{3N} \approx \frac{\sqrt{m_S^2 + p_z^2} + p_z}{m_N}, \tag{13}$$

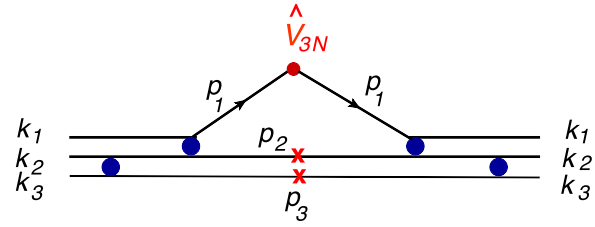

FIG. 4. The light-front diagram corresponding to the density matrix of 3N-SRCs. The 3N-SRCs here are due to successive pn short-range interactions. k_i and p_i are shorthand notations for the light-cone momenta $(\beta_i, k_{i,\perp})$ and $(\alpha_i, p_{i,\perp})$. The figure is adapted from Ref. [28].

we can calculate the longitudinal component of the initial momentum of the struck nucleon, p_z, which is the minimal possible momentum of the nucleon in 3N-SRC. According to the 3N-SRC scenario this momentum, p_z, is equal and opposite to the center-of-mass momentum of the recoil two-nucleon system. It is worth mentioning that this momentum does not appear directly in the argument of the light-cone nuclear wave function but enters through the nonlinear relation of Eq. (13). Nonetheless it gives an estimate of the bound nucleon momenta to be reached in a fixed target experiment aimed at probing 3N-SRCs. Figure 3(b) shows the dependence of $|p_z|$ on α_{3N}, with the arrows indicating the maximum possible α_{3N}'s that can be probed at given values of Q^2. One observes from the plot that the characteristic momenta of the struck nucleon in the 3N-SRCs for $\alpha_{3N} \geqslant 1.6$ is $p_z \gtrsim 700$ MeV/c.

III. DYNAMICS OF THE 3N-SRCs

In light of the recent observation of strong dominance of the pn component in 2N-SRCs [5,18,22] within the momentum range of 250–650 MeV/c and the assertion (discussed above) that type 3N-I SRCs dominate in inclusive scattering at $\alpha > 1.6$ and $|p_z| \gtrsim 0.7$ GeV/c, one expects that the main mechanism for generation of 3N-SRCs is due to successive pn short-range interactions [17,28,42] with the mass of the spectator 2N system tending to be small, $m_S \sim 2m_N$. Due to pn dominance 3N-SRCs should have predominantly ppn or nnp composition, with ppp and nnn configurations being strongly disfavored. The diagram representing the light-cone density matrix of 3N-SRCs is given in Fig. 4, where three-nucleon lines are ppn or nnp configurations. Calculation of the 3N-SRC contribution to the nuclear density matrix according to diagrams similar to Fig. 4 yields [28]

$$\begin{aligned}\rho_{3N}(\alpha_1) = \int \frac{1}{4}\Bigg[& \frac{3-\alpha_3}{(2-\alpha_3)^3}\rho_{pn}(\alpha_3, p_{3\perp}) \\ & \times \rho_{pn}\left(\frac{2\alpha_2}{3-\alpha_3}, p_{2\perp} + \frac{\alpha_1}{3-\alpha_3}p_{3\perp}\right) \\ & + \frac{3-\alpha_2}{(2-\alpha_2)^3}\rho_{pn}(\alpha_2, p_{2\perp}) \\ & \times \rho_{pn}\left(\frac{2\alpha_3}{3-\alpha_2}, p_{3\perp} + \frac{\alpha_1}{3-\alpha_2}p_{2\perp}\right)\Bigg]\end{aligned}$$

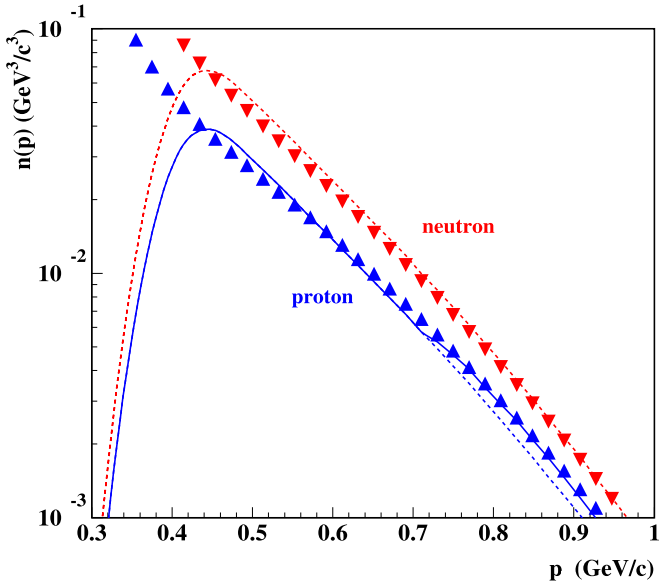

FIG. 5. The momentum distribution of the proton and neutron in ^{3}He. The triangle symbols are from the VMC calculation of Ref. [43]. The dashed lines are contributions from 2N SRCs only, solid lines correspond to the combined contributions from 2N and 3N SRCs [28]. In the case of the neutron distribution no 3N SRCs are included.

$$\times\,\delta\left(\sum_{i=1}^{3}\alpha_i - 3\right)$$
$$\times d\alpha_2 d^2p_{2\perp} d\alpha_3 d^2p_{3\perp}, \tag{14}$$

where $(\alpha_i, p_{i\perp})$ $(i = 1, 2, 3)$ are light-cone momentum fractions and transverse momenta of nucleons and $\rho_{pn}(\alpha, p_\perp)$ is the density matrix of pn-SRC. The prevalence of ρ_{3N} in a nuclear density function, ρ_A, in the 3N-SRC region suggests several characteristics that can be experimentally verified. One follows from Eq. (5), according to which $\rho_{pn} \sim a_2(A, z)\rho_d$, and therefore the per nucleon probability of finding a nucleon in a 3N-SRC, a_{3N}, should be proportional to the square of the probabilities of 2N SRCs, a_{2N} (actual relation will be given in Sec.V):

$$a_{3N}(A, Z) \sim a_{2N}(A, Z)^2. \tag{15}$$

Another feature follows from the expectation that the mass of the recoil 2N system, m_S, in 3N-SRC is small, which results in a small relative momentum in the recoiling NN system, $k = \frac{\sqrt{m_S^2 - 4m_N^2}}{2}$. The condition $k \ll m_N$ and the fact that isotriplet two-nucleon states with low relative momentum are strongly suppressed compared to the isosinglet states [19] produce a strong sensitivity of the 3N-SRCs on the isospin structure of NN recoil system. Namely, the dominant 3N-SRC configurations are those which have a recoil 2N system in the isosinglet state. This situation is illustrated in Fig. 5, where the high momentum distribution of protons and neutrons in ^{3}He, calculated in a variational Monte Carlo (VMC) approach [43], is compared with the calculation based on the 2N- and 3N-SRC model of Ref. [28], the latter being based on Eq. (14).

Figure 5 shows the 2N-SRC model completely describes the neutron momentum distribution up to 1 GeV/c, while one needs 3N-SRC contributions to describe the proton momentum distribution above 700 MeV/c. This result is in agreement with the dominance of isosinglet recoil NN systems in the generation of 3N-SRCs. For the case of the neutron, the recoil system is a pp pair, which is strongly suppressed as compared with that of the proton, in which case the recoil system is in the isosinglet pn state, where no suppression exists. Notice that even if the 3N-SRCs contribute to the proton momentum distribution in ^{3}He it is still a correction to the main 2N-SRC part of the momentum distribution as discussed in Sec. I.

It is worth mentioning that type 3N-II SRCs can be described through diagrams similar to Fig. 4, in which case the intermediate state between two successive NN interactions has a large invariant mass. Here another source of 3N-SRCs could be the configuration containing a Δ resonance in the intermediate state, which will represent the contribution from "genuine" three-nucleon forces irreducible to NN interactions. As discussed in Sec. II one expects that type 3N-I SRCs should be the dominant source of 3N correlations in inclusive reactions. Probing type 3N-II SRCs will require semi-inclusive processes in which the recoiling two-nucleon system has a large invariant mass.

IV. FINAL STATE INTERACTIONS

Final state interactions (FSI) can both distort and mimic 3N-SRCs. Detailed quantitative studies of the FSI effects are clearly necessary. Below we provide several qualitative considerations based on the high energy nature of electroproduction reactions which are used to probe 3N-SRCs. The main part here is that our interest is in LC momentum distribution function $\rho(\alpha_N)$, with α_N being the momentum fraction of nucleus carried by the interacting nucleon. The latter is analogous to the Bjorken-x, which is in deep-inelastic processes represents the LC momentum fraction of nucleon carried by the interacting quark. Our arguments related to the FSI are similar to that of DIS processes in which final state interaction of struck quark does not change the initial partonic distribution in the nucleon. In this respect, it can be shown that $\frac{\rho(\alpha)}{(2-\alpha)}$ is analogous to the partonic distribution function defined for the nucleon in the nucleus.

The 3N-SRC picture will be distorted mainly due to the multiple rescattering of nucleons from 3N-SRCs with the nucleons belonging to the "uncorrelated" spectator $(A-3)$ system. An example is presented in Fig. 6(a) in which a nucleon knocked out from a 3N-SRC rescatters off the uncorrelated nucleons in the $(A-3)$ residual nucleus. Other examples are the rescattering of spectator nucleons in the 3N-SRC with the uncorrelated nucleons from the $(A-3)$ system. For such rescatterings, because of inclusive nature of the process, one integrates over the range of excitation energies of the $(A-3)$ system. As a result the closure approximation can be applied (see discussion in Sec. II) which cancels the effects of long-range FSIs. The empirical evidence for such cancellation follows from the experimental observation of the 2N-SRC scaling in the $1 < x < 2$ domain [1–3,6] (also

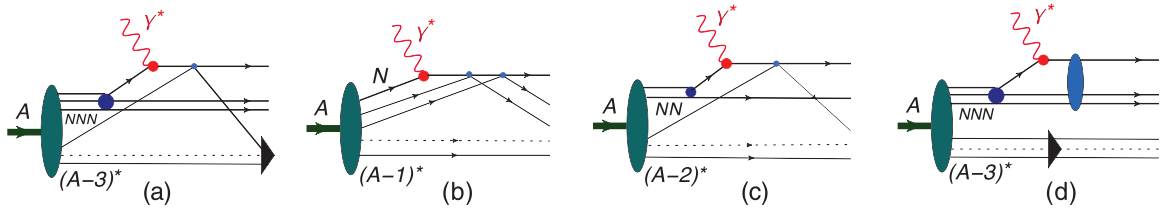

FIG. 6. Possible FSI diagrams contributing in 3N-SRC kinematics. Detailed description given in the text.

Sec. II) in which case the closure condition is satisfied for the FSI with the residual $(A-2)$ nucleus.

FSIs that can in principle mimic 3N-SRCs are diagrammatically presented in Figs. 6(b) and 6(c). In the case of (b) an uncorrelated nucleon in the mean field with initial LC momentum fraction, $\alpha_N \approx 1$, is struck and two successive rescatterings may increase the momentum faction to $\alpha_N \gtrsim 1.6$, making it appear as a nucleon from 3N-SRC. In the case of (c) a nucleon is knocked out from a 2N-SRC, where the characteristic momentum fraction is $1.3 \leqslant \alpha_N \leqslant 1.5$ and FSI shifts it to the $\alpha_N \gtrsim 1.6$ region. An important feature that suppresses the migration of a nucleon of modest α_N into the 3N-SRC region is the approximate conservation of the LC momentum fraction in the high energy (eikonal) regime of small angle rescattering [38,39]. In this case the nonconservation of α_N is estimated as [38,39]

$$\delta\alpha \approx \frac{x^2}{Q^2}\frac{2m_N E_R}{\left(1+\frac{4m_N^2x^2}{Q^2}\right)}, \tag{16}$$

where $E_R = \sqrt{m_S^2+p^2} - m_S$ and $p \approx 0.7-1$ GeV/c is the characteristic momentum of the nucleon in a 3N-SRC.

In Fig. 7 we present the Q^2 dependence of the nonconservation of α_N for $2 \leqslant x \leqslant 2.9$. The estimates are made for $p = 1$ GeV/c and $m_S = 2m_N$. It follows from the figure that

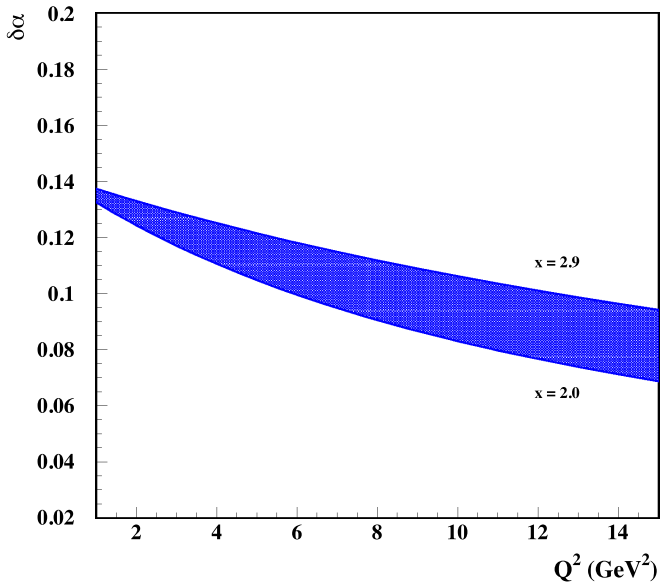

FIG. 7. Nonconservation of α_N as a function of Q^2 according to Eq. (16) for $p = 1$ GeV/c and $2 \leqslant x \leqslant 2.9$.

for $Q^2 > 3$ GeV^2 that FSI may alter α_N by no more than 0.14, which is too small to shift the mean field nucleon, $\alpha_N \approx 1$, to the 3N-SRC domain. However, one may expect possible FSI contributions from the 2N-SRC domain, $1.3 \leqslant \alpha_{2N} \leqslant 1.5$, influencing the onset of 3N-SRCs at $\alpha_{3N} \approx 1.6$.

Finally, the other FSI effects follow from the rescattering within a 3N-SRC as shown in Fig. 6(d). In this case one expects a modification of the $p_\perp$ distribution in the 3N-SRCs. However, the important feature of high energy small angle rescattering, discussed above, is that while FSI redistributes transverse momenta, it leaves the α_N distribution almost intact (see also Ref. [44]). As a result the measured inclusive cross section in the 3N-SRC domain can be presented in a factorized form similar to the 2N-SRC case [Eq. (4)]:

$$\sigma_{eA} \approx \sum_N \sigma_{eN}\rho_A^N(\alpha_{3N}), \tag{17}$$

where

$$\rho_A^N(\alpha_{3N}) = \int \rho_A^N(\alpha_{3N}, p_\perp)d^2p_\perp \tag{18}$$

is weakly modified due to FSI, even if the $p_\perp$ distribution of the unintegrated nuclear density matrix, $\rho_A^N(\alpha, p_\perp)$, is distorted by the FSI [44].

In the discussion above we focused only on the part of the FSI which corresponds to the pole contribution from the struck nucleon propagator, representing the on-shell propagation of the fast nucleon in the intermediate state. Another contribution to FSI comes from the nonpole term of the FSI amplitude, in which case the struck nucleon is highly virtual. There are two main sources of the suppression of the off-shell FSI contribution. First, the off-shell FSI contribution is proportional to the square of the real part of the NN scattering amplitude, which is smaller by an order of magnitude than the imaginary part (see, e.g., [45,46]). Second, due to the large virtuality of the fast nucleon the off-shell NN rescattering amplitude is strongly suppressed [47]. There is also empirical evidence from the studies of 2N-SRCs that off-shell rescattering amplitudes are negligible [1].

V. 3N-SRC OBSERVABLES

The experimental observation of 3N-SRCs is challenging for many reasons. As Fig. 5 shows, extracting the momentum distribution at $\gtrsim$700 MeV/c will not allow the isolation of 3N-SRCs due to substantial 2N-SRC contribution. Furthermore, the 3N-SRC contribution to the momentum distribution decreases faster with an increase of momentum than the 2N-SRC contribution. Overall, the bound nucleon momentum is

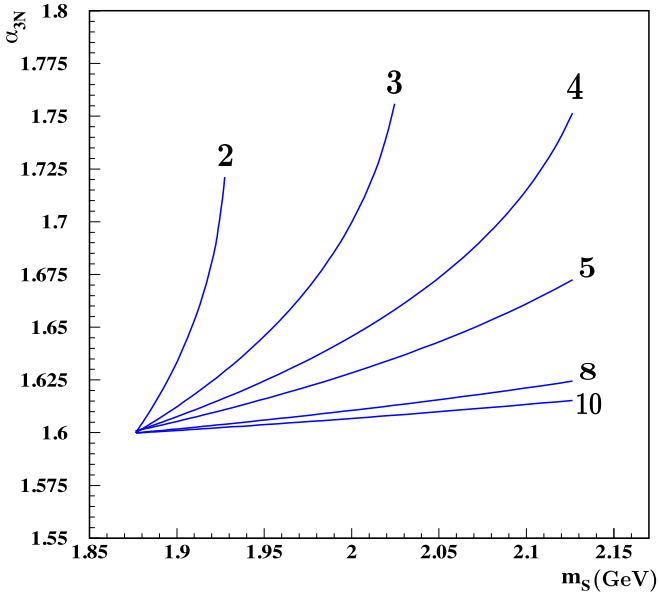

FIG. 8. Dependence of α_{3N} on the recoil mass, m_s, of the spectator system in 3N SRC for different values of Q^2, calculated according to Eq. (12).

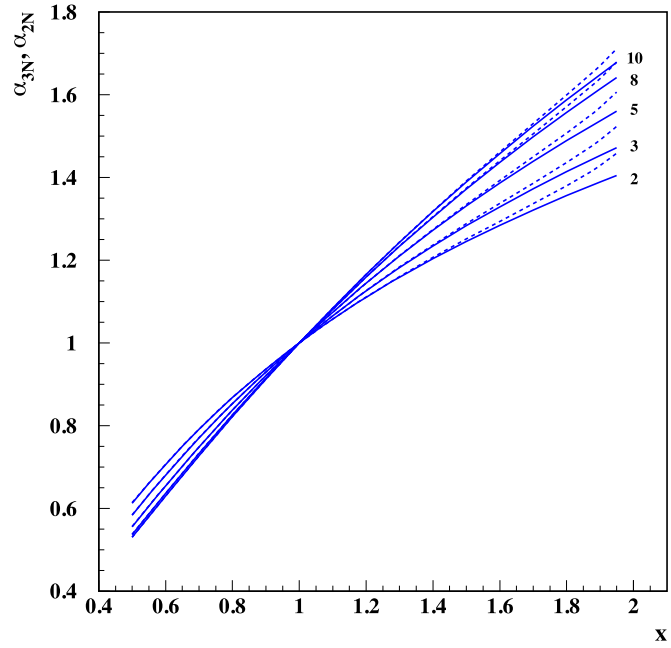

FIG. 9. The x dependence of α_{3N} (solid lines) and α_{2N} (dashed lines) at different Q^2.

not a good parameter with which to explore 3N-SRCs. The more natural parameter, as discussed earlier, is the light-cone momentum fraction α_N for which, according to Eq. (2), the condition $\alpha_N \gtrsim 2$ will completely isolate 3N-SRCs with the transition region expected to start at $\alpha_N \gtrsim 1.6$.

Moreover, according to Eq. (17) the cross section of inclusive reaction factorizes in the form of the product of electron-nucleon cross section and the $p_\perp$ integrated light-cone density matrix, $\rho_A(\alpha_{3N})$. Hence, the appropriate observable for 3N SRCs is the ratio of inclusive $A(e,e')X$ cross sections for nuclei A_2 and A_1 in the region of $\alpha_{3N} \geqslant \alpha^0_{3N}$ and $Q^2 > 3$ GeV^2:

$$R_{A_1}(A_2) = \left.\frac{A_1\sigma_{A_2}(x,Q^2)}{A_2\sigma_{A_1}(x,Q^2)}\right|_{\alpha_{3N}>\alpha^0_{3N}}. \tag{19}$$

In this case α^0_{3N} (expected to be $\approx$1.6) should be defined from the observation of the onset of a *plateau* in the α_{3N} dependence of the ratio $R_{A_1}(A_2)$. Note that in Eq. (19) the off-shell effects in electron–bound-nucleon scattering are mostly canceled in the ratio.

The observation of a plateau assumes also that α_{3N} is insensitive to the recoil mass of the spectator 2N system, m_S, over which the cross section of the inclusive scattering is integrated. This imposes an additional condition for the observation of scaling. This insensitivity is shown in Fig. 8 and is largely achieved at $Q^2 \geqslant 5$ GeV^2. However, the expectation that the integral over the recoil mass will saturate in the range of $2m_N \leqslant m_S \leqslant 2$ GeV [19] indicates a possibility of an early onset of the plateau already at $Q^2 = 3$ GeV^2.

In the region of $\alpha_{3N} < \alpha^0_{3N}$ at modest Q^2 ($\leqslant$3 GeV^2) one expects an existence of a pre-asymptotic domain where the ratios (19) are not constant as a function of α_{3N} but are largely Q^2 independent for fixed α_{3N}. This is mainly due to the factorization of the inclusive cross section in the form of Eq. (17).

Such a behavior would be analogous to the pattern observed for α_{2N} dependence of the ratio (5) at $\alpha_{2N} < 1.3$ [1]. This is reinforced in Fig. 9 where one observes that α_{2N} and α_{3N} are nearly identical for $x < 1.6$.

To connect the ratio $R_{A_1}(A_2)$, defined in Eq. (19), with theoretical calculations of nuclear density function we introduce parameter $a_3(A,Z)$ characterizing the probability of 3N SRCs for nearly symmetric nuclei as follows:

$$a_3(A,Z) = \frac{3}{A}\frac{\sigma_{eA}}{(\sigma_{e^3\mathrm{He}} + \sigma_{e^3\mathrm{H}})/2}. \tag{20}$$

This parameter can be related to the ratio $R_3(A,Z)$, which is defined in Eq. (19) for $A_2 = A$ and $A_1 = {}^3$He. The ratio $R_3(A,Z)$ is the most accessible experimental quantity.

Based on the factorization of Eq. (17), for $R_3(A,Z)$ and $a_3(A,Z)$ one obtains

$$R_3(A,Z) = a_3(A,Z)\frac{(\sigma_{ep}+\sigma_{en})/2}{(2\sigma_{ep}+\sigma_{en})/3}. \tag{21}$$

Thus, a measurement of the ratio $R_3(A,Z)$ will allow an extraction of the parameter $a_3(A,Z)$ which can be used for verification of the theoretical models of 3N SRCs.

Based on the above definitions we can also formulate an experimental observable which will allow us to verify the prediction of Eq. (15). For this, we notice that for type 3N-I SRC [Fig. 1(a)] the calculation of nuclear density function [28] [Eq. (14)] yields

$$a_3(A,Z) = \frac{a_2(A)^2}{a_2^p({}^3\mathrm{He})a_2^n({}^3\mathrm{He})}, \tag{22}$$

where a_2^p and a_2^n are per-nucleon probabilities of finding a proton or neutron in a 2N-SRC. One can relate these to the parameter $a_2(A,Z)$ of Eq. (5) using the estimate of high

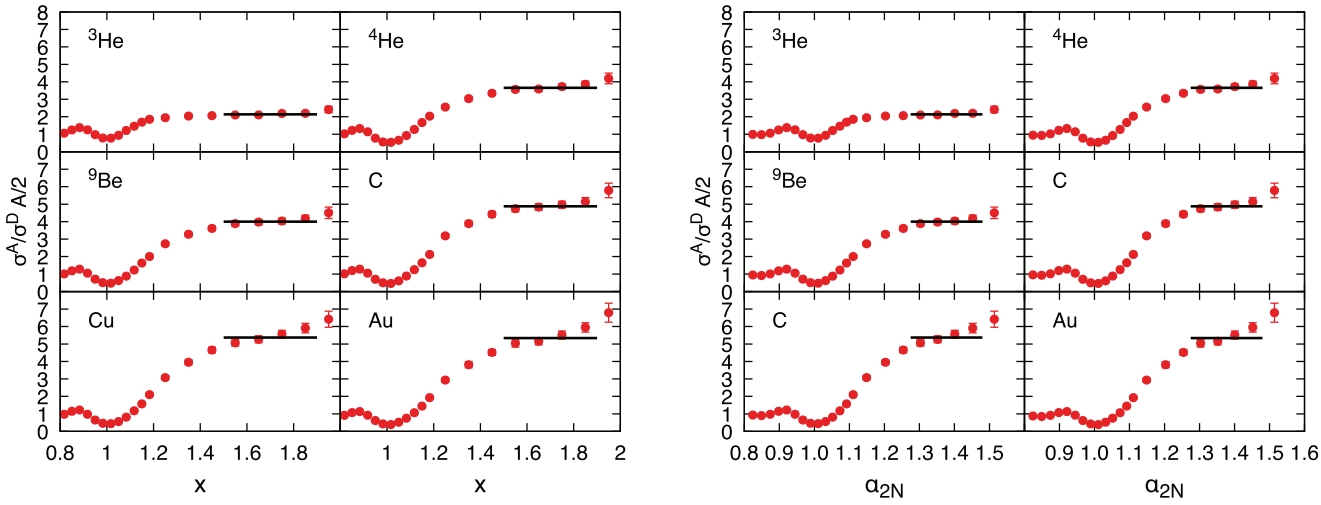

FIG. 10. Data from E02-019 [6,36] showing the ratios of $\frac{2\sigma_A}{A\sigma_D}$ against x and α_{2N} (right). The horizontal lines are the a_2 plateau values taken from [6].

momentum part of the proton and neutron distributions in nuclei within the *pn*-dominance model in the form [21]

$$n_2^{p/n}(p) = \frac{a_2(A)}{2(X^{p/n})^\gamma} n_d(p), \tag{23}$$

where $X^{p/n} = \frac{Z(N)}{A}$ is the relative fraction of the protons or neutrons and $n_d(p)$ is the high momentum distribution of the deuteron. According to Eq. (23) one estimates

$$a_2^n(^3\text{He}) = \frac{a_2(^3\text{He})}{2(1/3)^\gamma} \quad \text{and} \quad a_2^p(^3\text{He}) = \frac{a_2(^3\text{He})}{2(2/3)^\gamma}, \tag{24}$$

where $a_2(^3\text{He})$ is defined according to Eq. (5).

Using above estimates together with Eqs. (21) and (22) one obtains

$$\begin{aligned} R_3(A,Z) &= 4\left(\frac{2}{9}\right)^\gamma \frac{(\sigma_{ep}+\sigma_{en})/2}{(2\sigma_{ep}+\sigma_{en})/3}\left(\frac{a_2(A,Z)}{a_2(^3\text{He})}\right)^2 \\ &= 4\left(\frac{2}{9}\right)^\gamma \frac{(\sigma_{ep}+\sigma_{en})/2}{(2\sigma_{ep}+\sigma_{en})/3} R_2^2(A,Z), \end{aligned} \tag{25}$$

where in the last part of the equation we used the fact that the variables α_{2N} and α_{3N} have nearly same magnitudes in the 2N-SRC region (see Fig. 9) to relate the ratios of a_2 parameters to the experimentally measured ratio:

$$R_2(A,Z) = \frac{3}{A}\frac{\sigma_{eA}}{\sigma_{e^3\text{H}}}\Big|_{1.3<\alpha_{3N}<1.5} = \frac{a_2(A)}{a_2(^3\text{He})}. \tag{26}$$

In the following section we will analyze experimental data at $Q^2 \approx 3$ GeV^2 for which $\sigma_{ep} \approx 3\sigma_{en}$. This and using $\gamma \approx 0.85$ from Ref. [21] yields from Eq. (25)

$$R_3(A,Z) \approx 0.96 R_2(A,Z)^2 \approx R_2(A,Z)^2. \tag{27}$$

Equations (25) and (27) present a remarkable prediction: the ratios of inclusive nuclear cross sections (R_2 and R_3) measured in different domains of α_{3N} will be related by a simple quadratic relation if the scattering in the $\alpha_{3N} > \alpha_{3N}^0$ region probes type 3N-I SRCs.

VI. EXPERIMENTAL EVIDENCE FOR 3N-SRCs

Conclusive evidence for two-nucleon SRCs first appeared in 1993 [1] from the analysis of data from different experiments at SLAC. The SLAC data sets for light nuclei did not share common kinematics with the data for heavy nuclei [48] and it was necessary, after rebinning into common x bins, to interpolate the deuteron data across Q^2 to form the ratios of inclusive cross sections for nuclei A and the deuteron ($\frac{2\sigma_A}{A\sigma_D}$). The plateau for the available nuclei in these ratios had a weak A dependence for $A \geqslant 12$. The ratios were smaller for ^{3}He and ^{4}He (with large error bars). The $\frac{3\sigma_A}{A\sigma_{^3\text{He}}}$ ratios from Hall B at JLab showed similar plateaus [2,3]. These measurements provided persuasive evidence for the presence of 2N-SRCs yet were limited in their precision and/or the desired expansive range in x and Q^2. Most recently, experiment E02-019 [6,36] produced high quality data in the 2N-SRC region; these are reproduced in Fig. 10.

The data available to study 3N-SRCs are sorely limited. ^{3}He data (SLAC [15] and Hall B [2,3], Hall C [6], and Hall A [33] at Jefferson Lab) provided good agreement for the height of the 2N-SRC plateau for $x < 1.5 < 2.0$ yet there are significant disagreements in the $x > 2$ region. These arise from the fact that the SLAC data and data from Jefferson Lab's Hall A [33] are at the lower limit of the range of Q^2 necessary to study 3N correlations, and the same is true for a fraction of the data from CLAS [2,3]. The reliability of the observed scaling in the $x > 2$ region for CLAS data was questioned in Ref. [34], which observed that the modest momentum resolution of the CLAS detector in Hall B allows, when the cross sections are falling steeply with x, bin migration, in which events in a reconstructed x bin originated in a lower x bin. To get a sense for paucity of the data, we show in Fig. 11 the kinematic extent of all published ^{3}He data cited above as a scatter plot of Q^2 and x (top) and Q^2 and α_{3N} (bottom). As can be seen, only a small fraction of the data satisfy the necessary condition of $Q^2 \gtrsim 3$ GeV^2 and $\alpha_{3N} \gtrsim 1.6$, as indicated by the vertical line, even though the large set of data to the right of the vertical line at $x = 2$ in the top panel might suggest otherwise.

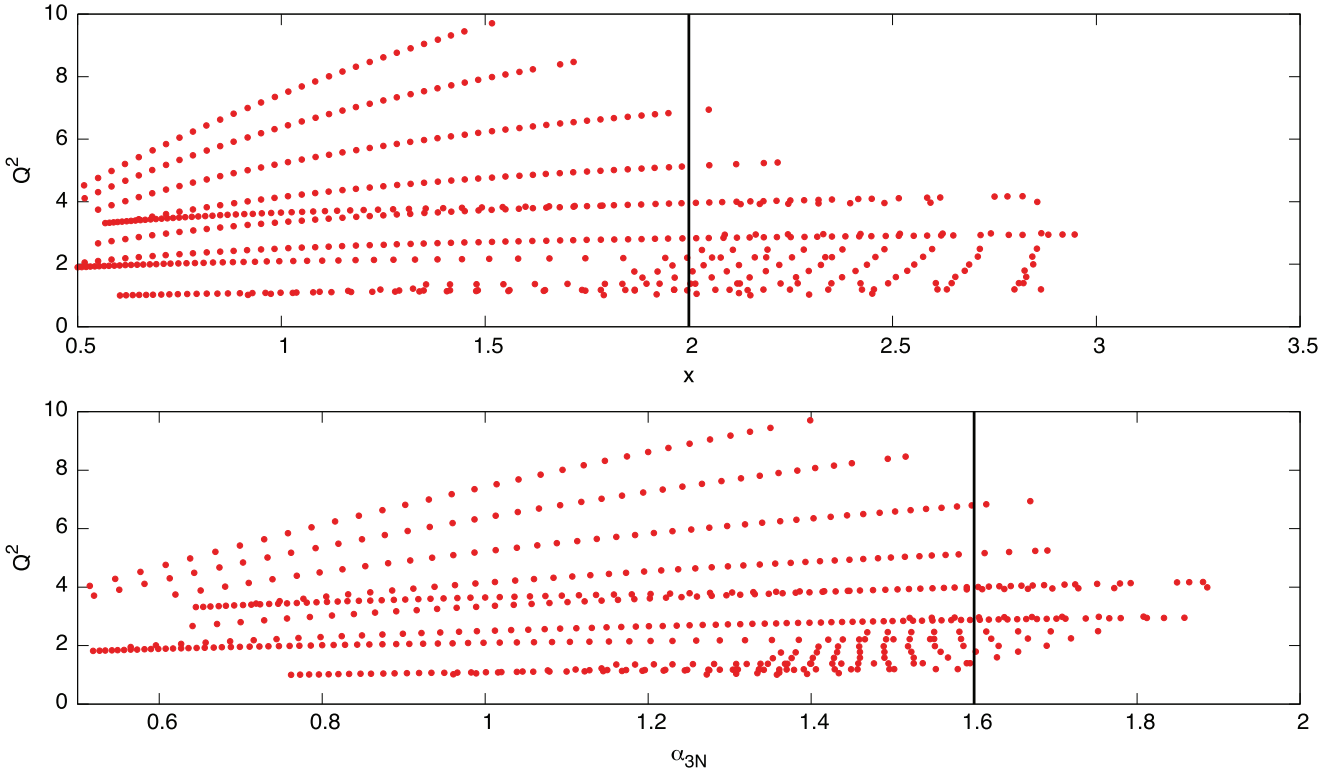

FIG. 11. Kinematic distribution of the world data set for ^{3}He with $Q^2 > 1$: Q^2 versus x (top) and Q^2 versus α_{3N} (bottom). Only data with $\alpha_{3N} > 1.6$ are used when considering 3N-SRC, as indicated by the black vertical line in the bottom panel. The kinematic points above do not necessarily imply corresponding data for other nuclei. It should be noted that at very large x and α_{3N} the data have large relative errors.

Experiment E02-109 [36,49–52] was developed with the goal, in part, to provide precision ratios, in the 2N-SRC region, at large momentum transfer for a wide range of nuclei. The ratios $\frac{2\sigma_A}{A\sigma_D}$ at $Q^2 \approx 2.75$ GeV^2 (at $x = 1$) indicated scaling patterns expected for the 2N-SRC region [6]. The heights of the plateaus at $x > 1.5$ scale approximately with A [6] (see Fig. 10) and have been related to the parameter $a_2(A, Z)$ [Eq. (5)] characterizing the probability of finding 2N-SRCs in nucleus A relative to the deuteron.

To check whether the α_{3N} description of the data results in the factorization implicit in Eq. (17), in Fig. 12 we compare the x and α_{3N} dependences of $\frac{3\sigma_A}{A\sigma_{^3\mathrm{He}}}$ for all available Q^2 from Refs. [6,36] for $A = 12$. As the comparison shows, the Q^2 spread of the data is significantly reduced once the ratios are evaluated in terms of α_{3N}, which absorbs part of the Q^2 dependence. The plateau in the region $1.3 < \alpha_{3N} < 1.5$ manifests the dominance of 2N-SRCs corresponding, here, to internal nucleon momenta in the range of 300–600 MeV/c. The plateaus arising from 2N-SRCs in the ratios as a function of α_{3N} (similarly to α_{2N}) can be seen as following from the fact (see Fig. 9) that numerically α_{2N} and α_{3N} have small differences at $Q^2 > 2$ GeV^2 and $x < 1.8$. The observation of 2N-SRCs in terms of α_{3N} is important for verifying the conjecture [Eq. (27)] that a plateau, if observed, in the 3N-SRC region should be proportional to $(\frac{a_2(A)}{a_2(^3\mathrm{He})})^2$.

As Fig. 12 shows, only the measurement at 18° [in which $Q^2 \simeq 2.5$ (GeV/c)^2 at the quasielastic peak, growing to $Q^2 \simeq 3$ (GeV/c)^2 at $x = 2.9$] reaches the region $\alpha_{3N} \simeq 1.6$ where one expects the onset of 3N-SRCs. It is intriguing that, as the lower panel of the figure shows at $\alpha_{3N} > 1.6$, the ratios indicate possible onset of the scaling. In further discussions, except where explicitly indicated, our analysis of [6] is limited to this data set.

Problems arose when constructing the ^{3}He cross section between $x = 2.68$ and $x = 2.85$ ($1.6 \leqslant \alpha_{3N} \leqslant 1.8$) due to difficulties with the subtraction of the walls of the aluminum target cell containing the ^{3}He. The limited vertex resolution of the spectrometer made it impossible to isolate electrons that scattered from the walls of the relatively small diameter (4 cm) target cell. This and the fact that $\sigma^{\mathrm{Al}} \gg \sigma^{^3\mathrm{He}}$ at large x, as $\sigma^{^3\mathrm{He}}$ must go to 0 at its kinematic limit, $x = 3$, resulted in a set of negative cross sections in three bins at large x mixed with other bins in which cross sections were consistent with zero with large relative errors.

In contrast, the data in the region below $x < 2.5$ are of excellent quality with small errors. As expected a y-scaling analysis [53,54] of the E02-019 data found it to be in good agreement with the SLAC data [12,15] from $y = 0$ (top of the quasielastic peak) to $y \simeq -1$ (GeV/c). In Fig. 13 we plot the scaling function $F(y)$ against y with the inset showing (in a linear scale) the region $-1.1 < y < -0.7$ and where the negative values of $F(y)$ arise from the negative ^{3}He cross sections mentioned above. Despite the negative ^{3}He cross sections the ratios $\frac{^4\mathrm{He}}{^3\mathrm{He}}$ over the entire x region from E02-019 were formed and published in Ref. [6] by making use of the following procedure. First, an inverted ratio, $\frac{^3\mathrm{He}}{^4\mathrm{He}}$, was formed

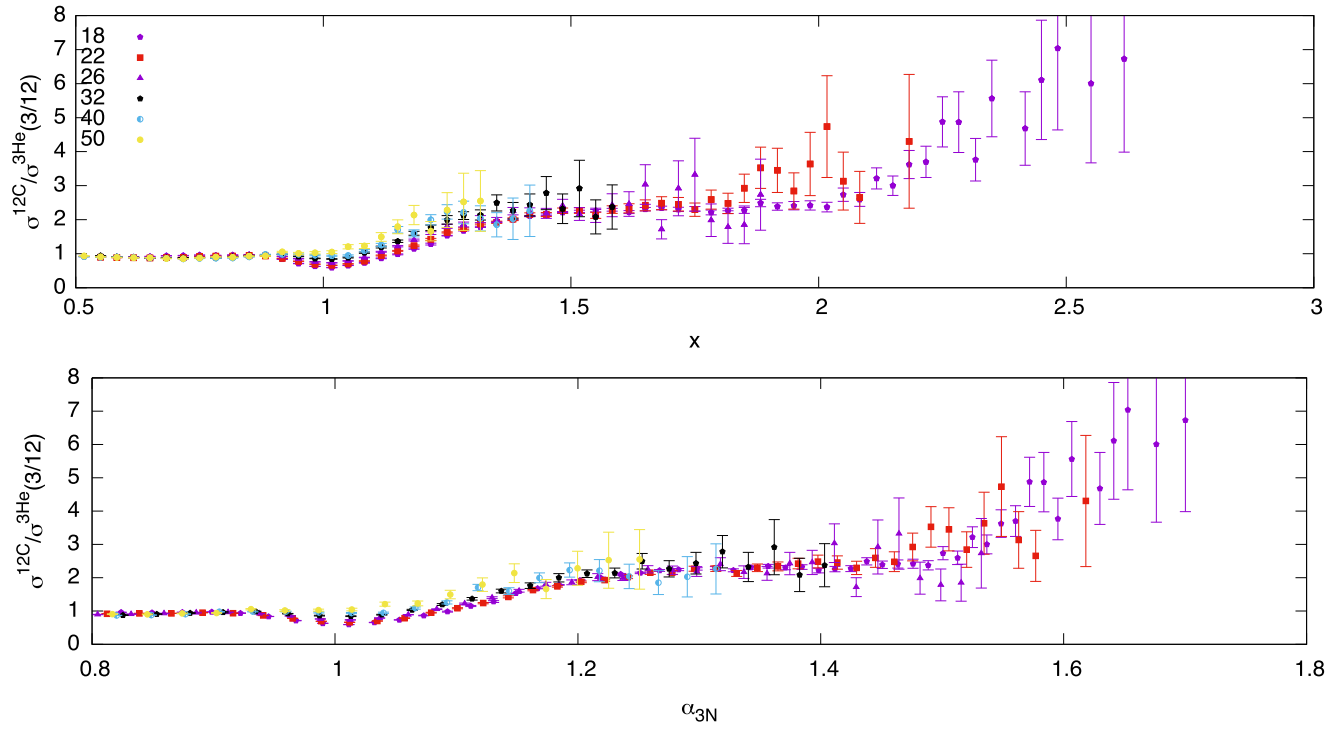

FIG. 12. The x and α_{3N} dependences of the per-nucleon ratios of ^{12}C / ^{3}He for different angles with Q^2 ranging 2.5–7.5 GeV^2 (at $x = 1$) against x (top) and α_{3N}. Only data with relative errors less than 0.5 are shown.

and then, for the region of $x \geqslant 1.15$, the data were rebinned by combining three bins into one, taking care of the error propagation. Subsequently the data in the inverted ratio that had error bars falling below zero were moved along a truncated Gaussian, such that the lower edge of the error bar was at zero. The result was then inverted to give the ratio $\frac{^4\text{He}}{^3\text{He}}$ shown in Fig. 3 of Ref. [6] and as the triangles in Fig. 14. The use of a truncated Gaussian gave rise to the asymmetric error bars seen in the ratio. A limitation of this approach is that it would have to be repeated for every nucleus when forming $\frac{\sigma^A}{\sigma^{^3\text{He}}}$.

As an alternative to the procedure of Ref. [6] we have used the following approach [35] to avoid the problematic ^{3}He data of Refs. [6,49,51] in the 3N-SRC region. We fit the y-scaling function $F(y)$, derived from the SLAC ^{3}He data between $x = 2.68$ and $x = 2.85$ ($1.6 \leqslant \alpha_{3N} \leqslant 1.8$). The fit was of the form $F(y) = a\exp(-by)$. We were then able to replace, point by

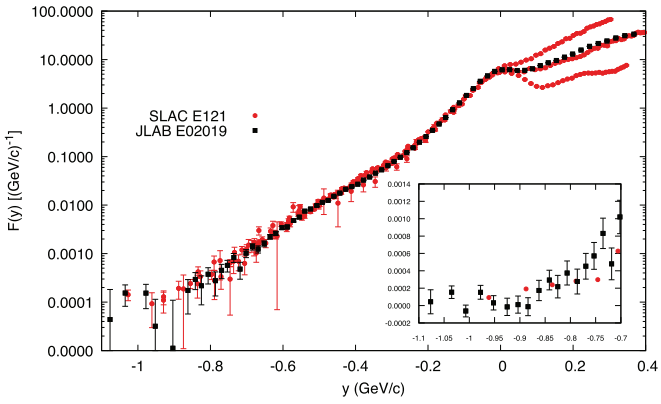

FIG. 13. $F(y)$ plotted against y for ^{3}He data from Refs. [6,12,15]. The inset shows $F(y)$ for $-0.7 > y > -1.1$. This corresponds to the region of interest for 3N-SRCs, $\alpha_{3N} \simeq 1.6$ (at $y = -0.7$) to $\alpha_{3N} \simeq 1.8$ (at $y = -1.1$). The selected SLAC data shown here have $1 < Q^2 < 4$ GeV/c^2. There is good agreement between the SLAC and Jefferson Lab data.

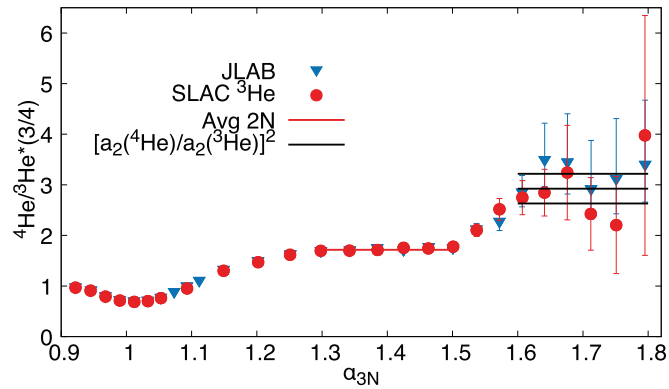

FIG. 14. The α_{3N} dependence of the inclusive cross section ratios for ^{4}He to ^{3}He. Triangles: JLAB data [6,49]; circles: ratios when using a parametrization of SLAC ^{3}He cross sections [12,15]. The horizontal line at $1.3 \leqslant \alpha_{3N} < 1.5$ identifies the magnitude of the 2N-SRC plateau. The line for $\alpha_{3N} > 1.6$ is Eq. (27) with a 10% error introduced to account for the systematic uncertainty in $a_2(A, Z)$ parameters across all measurements. The data correspond to $Q^2 \approx 2.5$ GeV^2 at $x = 1$, $\alpha_{3N} = 1$. The figure is adapted from Ref. [35].

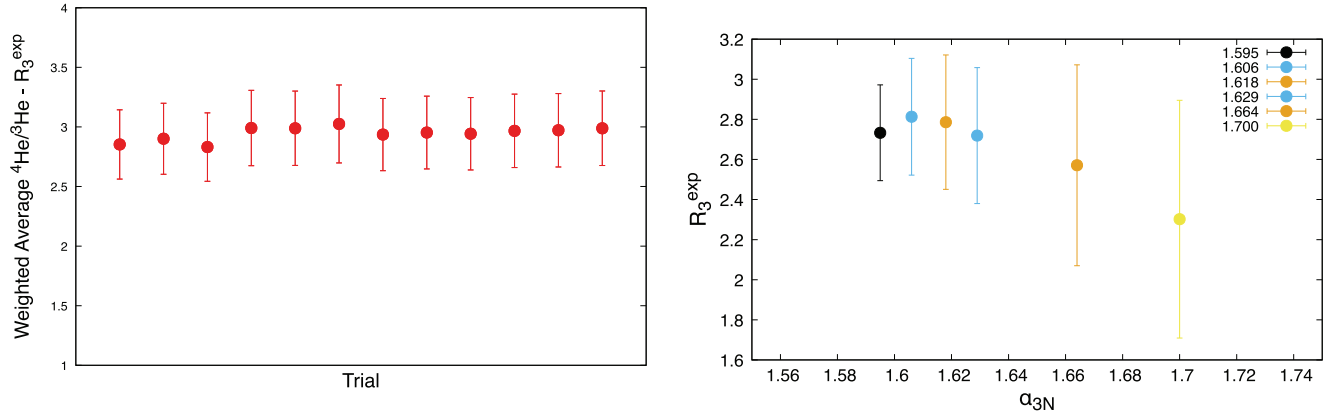

FIG. 15. Left: Sensitivity of ratio $\frac{^4\text{He}}{^3\text{He}}$ to the procedure of replacing the anomalous ^{3}He data for 12 different trials; four of the data sets used to form $F(y)$, including three sets for which fraction of the data have been replaced. Right: Sensitivity of the weighted average of $\frac{^4\text{He}}{^3\text{He}}$ in the 3N-SRC region to the lower limit of α_{3N}. The results shown in Fig. 17(a) remain unchanged within errors which grow with a larger $\alpha_{3N} > 1.6$ limit. In all cases (here and our final results) we restricted the upper limit such that W_{3N} was at least 50 MeV less than the elastic limit $\alpha_{3N} \leqslant 1.75$, $x \leqslant 2.85$, and $y \geqslant -0.92$ so as to avoid, as much as possible, FSI.

point, the ^{3}He cross sections from E02019 for which the central value was negative or its error bar fell below zero, through the following: $\frac{d^2\sigma}{d\Omega\, dE'} = \sum_{eN} \sigma_{eN} K F(y)$, where K is a kinematic factor and σ_{eN} is the elementary electron-nucleon cross section. The absolute error of the E02019 data set [6,49,51] was kept rather than the smaller errors from the fit. The fit parameters are $a = 0.296$ and $b = 8.241$. Note that a similar approach was used in Ref. [1], where the first evidence of 2N-SRCs through cross section ratios in inclusive scattering were revealed. Subsequently those results were confirmed by precision studies [2,3,6] in which the heavy and light cross section data were measured in single experiment.

Figure 14 presents the results for the cross section ratios obtained from the approaches described above: the one adopted in Ref. [6] (blue triangles) and another (red circles) in which the scaling function $F(y)$ is used to reconstruct cross sections between $x = 2.68$ and $x = 2.85$ ($1.6 \leqslant \alpha_{3N} \leqslant 1.8$). While the two approaches give similar results, we consider the replacement of the problematic data points as the best alternative procedure of Ref. [6] in part because it allows a consistent treatment of the ratios for all A.

Studies of systematics

We have worked to evaluate the sensitivity of the procedure above to obtain the $\frac{^4\text{He}}{^3\text{He}}$ ratios, as measured by R_3^{exp} [Eq. (19)], in multiple ways. We varied both the data sets used in the fit to $F(y)$ and the fraction of the data in the fit range, $-1.08 \geqslant y \leqslant -0.84$, that is replaced. We made fits to $F(y)$ built from four different data sets (1) the SLAC data only, (2) the JLAB data only, (3) both the JLAB and the SLAC data, and finally (4) the JLAB data absent its negative values. In addition, using the four fits to $F(y)$, we examined three variations of the fraction of the JLAB data set replaced by cross sections from the $F(y)$ fits: all the data in the fit range; just the six bins in the fit range where the data or its error bar went below zero; and only the data where the cross section values were negative. We found that these 12 variations for the ^{3}He cross sections resulted in weighted averages in the 3N region that agreed easily within their error bars. See Fig. 15. We show on the right-hand side of Fig. 15 the dependence of R_3^{exp} on the lower limit in α_{3N} when taking the weighted average. As can be seen, the result is not strongly dependent on α_{3N} and the error bars increase due to the worsening statistics.

Going back to Fig. 14 we notice that the plateau due to 2N-SRCs is clearly visible for $1.3 \leqslant \alpha_{3N} \leqslant 1.5$. In this region $\alpha_{3N} \approx \alpha_{2N}$, where α_{2N} is the LC momentum fraction of the nucleon in the 2N-SRC. Because of this, we refer to the magnitude of this plateau as $R_2(A, Z)$, defined in Eq. (26).

The horizontal line in the region of $1.3 \leqslant \alpha_{3N} \leqslant 1.5$ is given by the right-hand side of Eq. (26), in which the values of $a_2(^3\text{He})$ and $a_2(A)$ are taken from the last column of Table II in Ref. [55], an average of the SLAC, JLAB Hall C, and JLAB Hall B results. The magnitude of the horizontal solid line in the region of $1.6 \leqslant \alpha_{3N} \leqslant 1.8$ is the prediction of $R_{3N}(A, Z) \approx R_{2N}^2(A, Z)$, which was explained in the previous section [Eq. (27)]. We assigned a 10% error to this prediction (dashed lines) related to the uncertainty of $a_2(A, Z)$ magnitudes across different measurements.

With the same ^{3}He cross sections in Fig. 16 we evaluated ratios of cross sections $\frac{3\sigma^A}{A\sigma^{^3\text{He}}}$ for the nuclei (^{4}He, ^{9}Be, ^{12}C, ^{64}Cu, and ^{197}Au). Additionally in this figure we evaluated the magnitudes of $\frac{a_2(A)}{a_2(^3\text{He})}$ (taken from Ref. [6]) which are indicated by horizontal lines for $1.3 \leqslant \alpha_{3N} \leqslant 1.5$, where the plateau due to 2N-SRCs is observed.

As can be seen from these figures, despite large errors, the data (similar to Fig. 14) indicate a strong enhancement in the ratio $R_3(A)$ as soon as $\alpha_{3N} \gtrsim 1.6$, and are in qualitative agreement with the prediction of Eq. (27). To test quantitatively the prediction of Eq. (27), in Fig. 17(a) we evaluated the weighted average of $R_3^{exp}(A, Z)$ for $\alpha_{3N} > 1.6$ and compared them with the magnitude of $(\frac{a_2(A,Z)}{a_2(^3\text{He})})^2$ in which $a_2(A, Z)$'s are taken from Ref. [55]. In these evaluations ^{3}He cross sections were taken from the $F(y)$ fit to the SLAC data. Numerical data of Fig. 17 are presented also Table I. The comparison in Fig. 17(a)

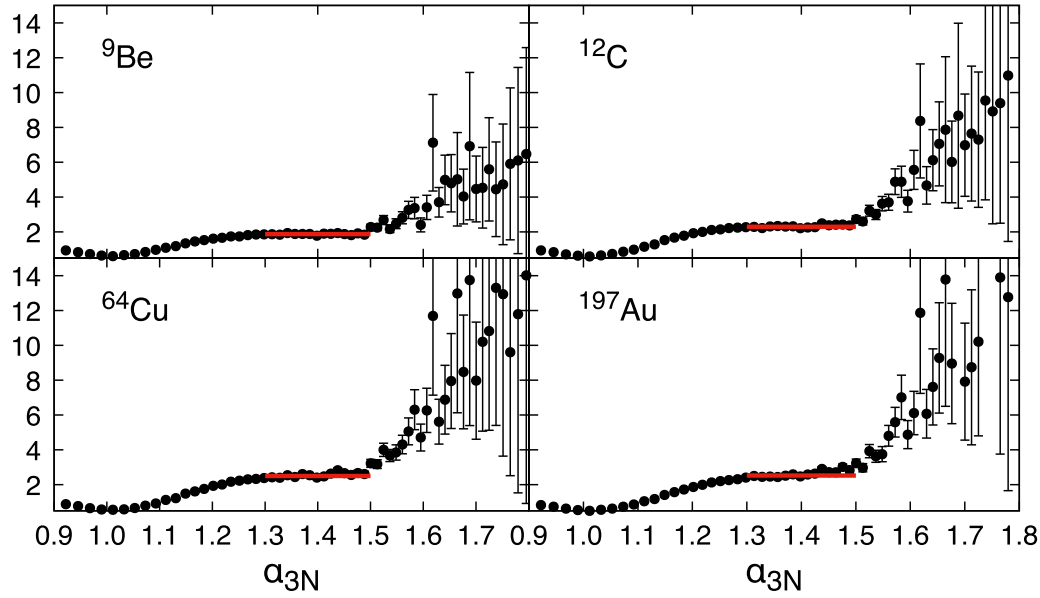

FIG. 16. Per-nucleon cross section ratios for ^{9}Be, ^{12}C, ^{64}Cu, ^{197}Au to ^{3}He. Horizontal lines indicate $\frac{a_2(A)}{a_2(^3\mathrm{He})}$ in the 2N-SRC region.

shows good agreement with the prediction of Eq. (27) for the full range of nuclei. We investigated the sensitivity of the weighted average of $R_3(A, Z)$ on the lower limit of α_{3N} (before rebinning) and found that the results shown in Fig. 17(a) remain unchanged within errors which grow with a larger $\alpha_{3N} > 1.6$ cut.

The agreement presented in Fig. 17(a) represents the strongest evidence yet for the presence of 3N-SRCs. If it is indeed due to the onset of 3N-SRCs then one can use the measured R_3^{exp} ratios and Eq. (21) to extract the $a_3(A, Z)$ parameters characterizing the 3N-SRC probabilities in the nuclear ground state. The estimates of $a_3(A, Z)$ and comparisons with $a_2(A, Z)$ are given in Fig. 17(b) (see also Table I). These comparisons show a faster rise for $a_3(A, Z)$ with A, consistent with the expectation of the increased sensitivity of 3N-SRCs to the local nuclear density [32]. If this result is verified in the future with better quality data and a wider range of nuclei then the evaluation of the parameter $a_3(A, Z)$ as a function of nuclear density and proton-neutron asymmetry together with $a_2(A, Z)$ can provide an important theoretical input for the exploration of the dynamics of superdense nuclear matter (see, e.g., [56]).

VII. SUMMARY AND OUTLOOK

We determined the kinematic conditions for isolating 3N-SRCs in inclusive $A(e, e')X$ reactions at large x. Based on the analysis of short-range structure of ^{3}He nuclei we expect that the dominant mechanism of 3N-SRCs in inclusive processes is due to three-nucleon correlations, in which one fast nucleon is balanced by two spectator nucleons with rather small invariant mass, $2m_N \leqslant m_S \lesssim 1.9$ GeV. Momenta of all three nucleons, however, exceed the characteristic Fermi momentum of the nucleus, $k_F \approx 250$ MeV/c. We referred such correlations as type 3N-I SRCs.

We explain that due to the specific nature of the high momentum components of the nuclear wave functions, the momentum of the fast nucleon is not the optimal variable

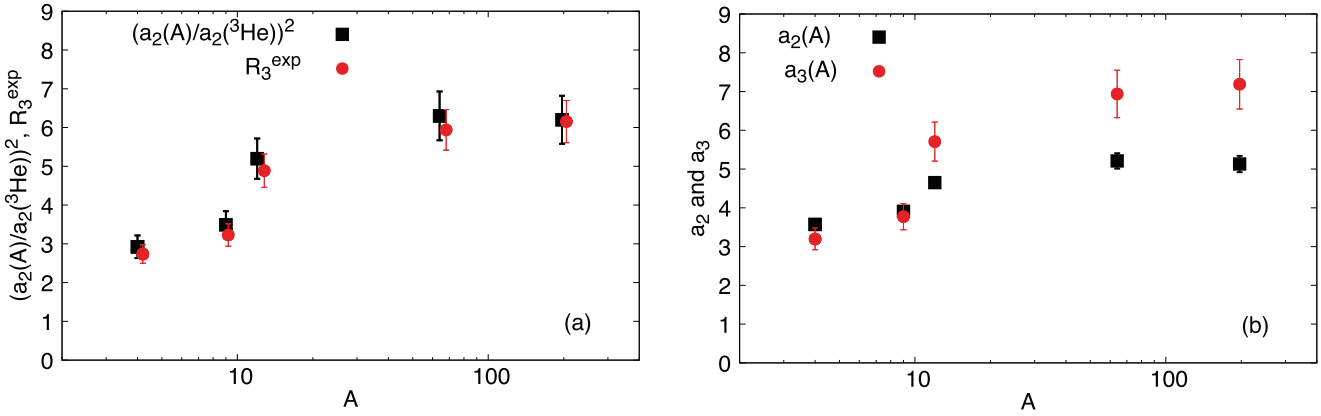

FIG. 17. (a) The A dependence of the experimental evaluation of R_3 compared with the prediction of Eq. (27). (b) The A dependence of $a_3(A, Z)$ parameter compared to $a_2(A, Z)$ of Ref. [6].

TABLE I. Numerical values a_2 [55], R_2 [Eq. (26)], $R_3^{\rm exp}$ (the weighted average in the 3N region), and a_3 calculated from Eq. (21).

A	a_2	R_2	$R_3^{\rm exp}$	a_3
3	2.13 ± 0.04	1	NA	NA
4	3.57 ± 0.09	1.68 ± 0.03	2.74 ± 0.24	3.20 ± 0.28
9	3.91 ± 0.12	1.84 ± 0.04	3.23 ± 0.29	3.77 ± 0.34
12	4.65 ± 0.14	2.18 ± 0.04	4.89 ± 0.43	$5.71 \pm 0, 50$
64	5.21 ± 0.20	2.45 ± 0.04	$(5.94 \pm 0.52$	6.94 ± 0.77
197	5.13 ± 0.21	2.41 ± 0.05	6.15 ± 0.55	7.18 ± 0.64

for the analysis since it does not allow the separation of 2N- and 3N-SRCs. In this respect the light-cone momentum fraction of 3N-SRC carried by the interacting nucleon, α_{3N}, is more suitable and existing phenomenology indicates that the onset of the 3N-SRC dominance is expected at $\alpha_{3N} > 1.6$. We derived the expression for α_{3N} for inclusive $A(e, e')X$ processes and demonstrated that the $\alpha_{3N} \gtrsim 1.6$ condition puts a strong constraint on Q^2 of the reaction, requiring $Q^2 \gtrsim 3$ GeV^2. Under these conditions we expect that the dominance of 3N-SRCs will lead to a plateau for per-nucleon inclusive cross section ratios of heavy to light nuclei. This will be in addition to the plateau observed in the 2N-SRC region.

Furthermore, based on the *pn* dominance in 2N-SRCs we predict that 3N-SRCs are generated through two successive *pn* short-range interactions. Within such a scenario we derived a quadratic relation between per nucleon ratios of nuclear and ^{3}He inclusive cross sections measured in the 2N- (R_2) and 3N- (R_3) SRC regions: $R_3 \approx R_2^2$.

We analyzed the existing inclusive data under the above conditions and found an indication for the onset of the plateau at $\alpha_{3N} > 1.6$. It is very intriguing that the magnitude of the plateau, R_3, is in agreement with predicted $R_3 \approx R_2^2 \approx (\frac{a_2(A)}{a_2(^3\text{He})})^2$ dependence. This agreement allowed us to extract per-nucleon probabilities, $a_3(A, Z)$ of finding 3N-SRCs in nuclei A relative to the ^{3}He nucleus.

The forthcoming experiments at Jefferson Lab will be able to significantly improve the current experimental situation. One important condition is that such experiments will be able to cover a larger Q^2 region. As Fig. 18 shows an increase of Q^2 will significantly widen the range of the α_{3N} accessible by the experiment. It is worth mentioning that at $Q^2 \gtrsim 5$ (GeV/c)^2 one will be able to cross to the $\alpha_{3N} \geqslant 2$ region, where one expects maximal contribution due to 3N-SRCs.

It is with anticipation that we await the running and analysis of Jefferson Lab's E1206-105 [57] experiment which has multiple goals: to measure cross sections (1) from light nuclei to compare to *ab initio* calculations and to study FSI; (2) from nuclei at low and moderate Q^2 with a range of *p-n* asymmetries in order to look for isospin dependence in the per-nucleon ratios; (3) at moderate Q^2 and large x to search for definitive evidence to 3N-SRCs; and finally (4) at very large Q^2 to look for the transition from quasielastic to deep inelastic scattering from nuclei as part of an effort to extract nuclear parton distribution functions at $x > 1$. The lines in Fig. 18 indicate the tentative range in Q^2 and α_{3N} which will be part of the goal of this experiment in studying 3N SRCs.

Finally, type 3N-I SRCs the discussed in this work correspond to those states in superdense nuclear matter in which no inelastic transition took place in the intermediate states. To investigate type 3N-II SRCs that are sensitive to irreducible 3N nuclear forces containing inelastic transitions one will need studies of semi-inclusive processes in which nucleons from 3N-SRCs are detected in coincidence with scattered electrons. In particular, it would be instructive to compare production from 3N system in different isospin states, such as three protons, where contribution of the repulsive core is enhanced, and the $2p + n$ state, in which the attraction dominates.

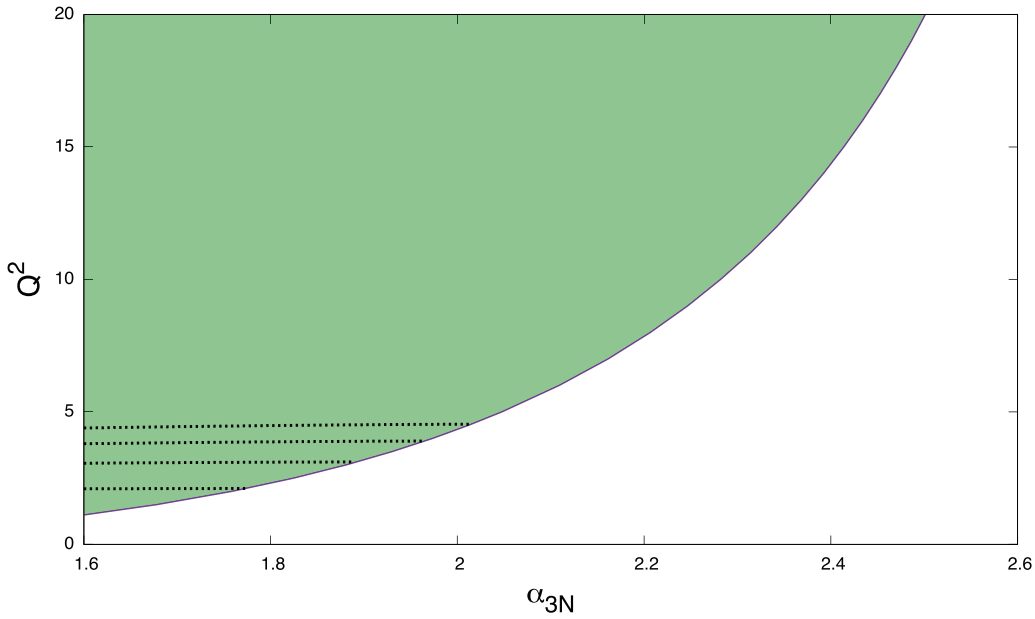

FIG. 18. The Q^2 range necessary in order to isolate 3N-SRCs. Also shown is the kinematic extent of an upcoming 12 GeV experiment [57].

ACKNOWLEDGMENTS

This work was supported in part by the DOE Office of Science, Office of Nuclear Physics, Contracts No. DE-FG02-96ER40950 (D.B.D.), No. DE-FG02-93ER40771 (M.I.S.), and No. DE-FG02-01ER41172 (M.S.S.).

[1] L. L. Frankfurt, M. I. Strikman, D. B. Day, and M. Sargsyan, Phys. Rev. C **48**, 2451 (1993).
[2] K. S. Egiyan *et al.* (CLAS Collaboration), Phys. Rev. C **68**, 014313 (2003).
[3] K. S. Egiyan *et al.* (CLAS Collaboration), Phys. Rev. Lett. **96**, 082501 (2006).
[4] R. Shneor *et al.* (Jefferson Lab Hall A Collaboration), Phys. Rev. Lett. **99**, 072501 (2007).
[5] R. Subedi, R. Shneor, P. Monaghan, B. D. Anderson, K. Aniol, J. Annand, J. Arrington and H. Benaoum *et al.*, Science **320**, 1476 (2008).
[6] N. Fomin, J. Arrington, R. Asaturyan, F. Benmokhtar, W. Boeglin, P. Bosted, A. Bruell and M. H. S. Bukhari *et al.*, Phys. Rev. Lett. **108**, 092502 (2012).
[7] J. Arrington, D. W. Higinbotham, G. Rosner, and M. Sargsian, Prog. Part. Nucl. Phys. **67**, 898 (2012).
[8] J. L. S. Aclander *et al.*, Phys. Lett. B **453**, 211 (1999).
[9] A. Tang *et al.*, Phys. Rev. Lett. **90**, 042301 (2003).
[10] S. Rock, R.G. Arnold, P. Bosted, B.T. Chertok, B.A. Mecking, I. Schmidt, Z.M. Szalata, R.C. York, and R. Zdarko, Phys. Rev. Lett. **49**, 1139 (1982).
[11] R. G. Arnold *et al.*, Phys. Rev. Lett. **61**, 806 (1988).
[12] D. Day *et al.*, Phys. Rev. Lett. **43**, 1143 (1979).
[13] D. B. Day *et al.*, Phys. Rev. Lett. **59**, 427 (1987).
[14] W. P. Schütz *et al.*, Phys. Rev. Lett. **38**, 259 (1977).
[15] S. Rock *et al.*, Phys. Rev. C **26**, 1592 (1982).
[16] I. Yaron, L. Frankfurt, E. Piasetzky, M. Sargsian, and M. Strikman, Phys. Rev. C **66**, 024601 (2002).
[17] L. L. Frankfurt and M. I. Strikman, Phys. Rep. **76**, 215 (1981).
[18] E. Piasetzky, M. Sargsian, L. Frankfurt, M. Strikman, and J. W. Watson, Phys. Rev. Lett. **97**, 162504 (2006).
[19] M. M. Sargsian, T. V. Abrahamyan, M. I. Strikman, and L. L. Frankfurt, Phys. Rev. C **71**, 044615 (2005).
[20] R. Schiavilla, R. B. Wiringa, S. C. Pieper, and J. Carlson, Phys. Rev. Lett. **98**, 132501 (2007).
[21] M. M. Sargsian, Phys. Rev. C **89**, 034305 (2014).
[22] O. Hen, M. Sargsian, L. B. Weinstein, E. Piasetzky, H. Hakobyan, D. W. Higinbotham, M. Braverman and W. K. Brooks *et al.*, Science **346**, 614 (2014).
[23] M. Duer *et al.* (CLAS Collaboration), Phys. Rev. Lett. **122**, 172502 (2019).
[24] M. Duer *et al.* (CLAS Collaboration), Nature **560**, 617 (2018).
[25] C. Ciofi degli Atti, S. Simula, L. L. Frankfurt, and M. I. Strikman, Phys. Rev. C **44**, R7 (1991).
[26] C. Ciofi degli Atti and S. Simula, Phys. Rev. C **53**, 1689 (1996).
[27] J. Ryckebusch, M. Vanhalst, and W. Cosyn, J. Phys. G: Nucl. Part. Phys. **42**, 055104 (2015).
[28] O. Artiles and M. M. Sargsian, Phys. Rev. C **94**, 064318 (2016).
[29] C. Ciofi degli Atti, C. B. Mezzetti and H. Morita, Phys. Rev. C **95**, 044327 (2017).
[30] H. Heiselberg and V. Pandharipande, Annu. Rev. Nucl. Part. Sci. **50**, 481 (2000).
[31] N. Fomin, D. Higinbotham, M. Sargsian, and P. Solvignon, Annu. Rev. Nucl. Part. Sci. **67**, 129 (2017).
[32] L. Frankfurt, M. Sargsian, and M. Strikman, Int. J. Mod. Phys. A **23**, 2991 (2008).
[33] Z. Ye *et al.* (The Jefferson Lab Hall A Collaboration), Phys. Rev. C **97**, 065204 (2018).
[34] D. W. Higinbotham and O. Hen, Phys. Rev. Lett. **114**, 169201 (2015).
[35] M. M. Sargsian, D. B. Day, L. L. Frankfurt, and M. I. Strikman, Phys. Rev. C **100**, 044320 (2019).
[36] N. Fomin, Inclusive scattering from nuclei in the quasielastic region at large momentum transfer, Ph.D. thesis, University of Virginia, 2008.
[37] L. L. Frankfurt and M. I. Strikman, Phys. Rep. **160**, 235 (1988).
[38] M. M. Sargsian, Int. J. Mod. Phys. E **10**, 405 (2001).
[39] L. L. Frankfurt, M. M. Sargsian, and M. I. Strikman, Phys. Rev. C **56**, 1124 (1997).
[40] M. M. Sargsian, T. V. Abrahamyan, M. I. Strikman, and L. L. Frankfurt, Phys. Rev. C **71**, 044614 (2005).
[41] A. Nogga, A. Kievsky, H. Kamada, W. Glöckle, L. E. Marcucci, S. Rosati, and M. Viviani, Phys. Rev. C **67**, 034004 (2003).
[42] A. J. Freese, M. M. Sargsian and M. I. Strikman, Eur. Phys. J. C **75**, 534 (2015).
[43] R. B. Wiringa, R. Schiavilla, S. C. Pieper and J. Carlson, Phys. Rev. C **89**, 024305 (2014).
[44] W. Boeglin and M. Sargsian, Int. J. Mod. Phys. E **24**, 1530003 (2015).
[45] W. Cosyn and M. Sargsian, Int. J. Mod. Phys. E **26**, 1730004 (2017).
[46] W. Cosyn, W. Melnitchouk and M. Sargsian, Phys. Rev. C **89**, 014612 (2014).
[47] M. M. Sargsian, Phys. Rev. C **82**, 014612 (2010).
[48] D. B. Day *et al.*, Phys. Rev. C **48**, 1849 (1993).
[49] N. Fomin *et al.*, Phys. Rev. Lett. **105**, 212502 (2010).
[50] N. Fomin, in *VII Latin American Symposium on Nuclear Physics and Applications, 11–16 June 2007, Cusco* (Peru), edited by R. Alarcon, P. L. Cole, C. Djalali, and F. Umeres, AIP Conf. Proc. No. 947 (AIP, New York, 2007), p. 174.
[51] J. Arrington, D. Day, A. Lung, and B. Filippone (spokespersons), Inclusive scattering from nuclei at $x > 1$ and high Q^2 with a 6 GeV beam, Jefferson Lab Experiment No. E-02-019, 2002 (unpublished).
[52] N. Fomin (private communication).
[53] D. B. Day, J. S. McCarthy, T. W. Donnelly, and I. Sick, Annu. Rev. Nucl. Part. Sci. **40**, 357 (1990).
[54] I. Sick, D. Day, and J. S. McCarthy, Phys. Rev. Lett. **45**, 871 (1980).
[55] J. Arrington, A. Daniel, D. B. Day, N. Fomin, D. Gaskell, and P. Solvignon, Phys. Rev. C **86**, 065204 (2012).
[56] D. Ding, A. Rios, H. Dussan, W. H. Dickhoff, S. J. Witte, A. Carbone, and A. Polls, Phys. Rev. C **94**, 025802 (2016).
[57] J. Arrington and D. Day (spokespersons), Inclusive scattering from nuclei at $x > 1$ in the quasielastic and deeply inelastic regimes, Jefferson Lab Experiment No. E12-06-105, 2006 (unpublished).